Journal of Rock Mechanics and Geotechnical Engineering 17 (2025) 7172–7182

Contents lists available at ScienceDirect

Journal of Rock Mechanics and Geotechnical Engineering

journal homepage: www.jrmge.cn

Full Length Article

Effects of normal stress and shear velocity on the frictional healing behavior of halite fault gouge

Junjie Wei [a, b], Tuo Wang [c, *], Fengshou Zhang [a, b]

[a] Key Laboratory of Geotechnical and Underground Engineering of the Ministry of Education, Tongji University, Shanghai, 200092, China
[b] Department of Geotechnical Engineering, Tongji University, Shanghai, 200092, China
[c] Department of Civil and Environmental Engineering, The Hong Kong Polytechnic University, Hong Kong, 100872, China

ARTICLE INFO

Article history:
Received 31 July 2024
Received in revised form
8 January 2025
Accepted 12 February 2025
Available online 2 May 2025

Keywords:
Halite gouge
Frictional healing
Induced earthquake
Normal stress
Shear velocity
Changning area

ABSTRACT

The distinctive characteristics exhibited by the aftershocks of *Ms*6.0 induced earthquakes in Changning, Sichuan, China, have attracted significant attention. The prevalence of salt rock (halite) in this area is closely associated with induced seismic events. The present study was conducted to examine the role of halite in frictional properties. To this end, laboratory measurements were taken for simulated fault gouge composed of halite. Slide-hold-slide (SHS) shear experiments were performed on gouges with grain size <106 μm at constant normal stress from 5 MPa to 30 MPa and constant shear velocity in the range of 1 −10 μm/s. Halite gouge shows higher frictional strength and frictional healing rate than most minerals. The results reveal that the fault within halite can potentially generate intense seismic events and more significant aftershocks. An increase in normal stress leads to a reduction in frictional healing, with frictional strength initially increasing and then decreasing. The elevated shear velocity following fault activation facilitates fault dilation, diminishes the frictional strength of the fault, and contributes to fault healing during the inter-seismic period. The aforementioned findings will contribute to a comprehensive understanding of the potential for the healing property of induced seismicity on faults containing halite, particularly in the Changning region of China.

© 2025 Institute of Rock and Soil Mechanics, Chinese Academy of Sciences. Published by Elsevier B.V. This is an open access article under the CC BY license (http://creativecommons.org/licenses/by/4.0/).

1. Introduction

The occurrence of induced seismicity, resulting from human activities such as salt mining, unconventional resource recovery, CO_2 geological storage, waste and nuclear disposal, and geothermal reservoir stimulation, has raised significant public concerns (Ellsworth, 2013; Atkinson et al., 2020; Schultz et al., 2020; Snæbjörnsdóttir et al., 2020; Li et al., 2024). In recent years, there has been a marked increase in moderate to strong earthquakes in southeastern Sichuan, China, culminating in an *Ms*6.0 earthquake in Changning in 2019 – the largest induced earthquake recorded in the region (Fig. 1). The epicenter of the *Ms*6.0 earthquake was proximate to the Shuanghe Salt Mine in Changning County (Lei et al., 2019). He et al. (2019) identified a salt rock layer approximately 240 m thick beneath the Lower Cambrian Dengying Formation at a depth of around 3000 m, directly beneath the operational area of the salt mine, which has been used for several decades. Before the initiation of salt mining activities, seismic activity in the region was relatively subdued. However, following the onset of salt mining and associated water injection operations, a noticeable increase in both the magnitude and frequency of earthquakes was observed. This escalation in seismic activity was strongly correlated with the volume of water loss during the salt mining process (Sun et al., 2017). Further studies have identified that the Changning *Ms*6.0 earthquake is linked with low V_P, low V_S, and high V_P/V_S values in this area, indicating that the earthquake may be attributed to water loss during the salt mining process (Zhang et al., 2020; Anyiam et al., 2024). The diffusion of these fluids may have augmented pore pressure in the shallow crust layers, which, along with differential subsidence resulting from salt mining activities and the presence of highly fractured, silica-enriched, slip-prone rocks, precipitated these earthquakes (Li et al., 2023; Anyiam et al., 2024). Consequently, a significant correlation has been asserted between salt mining activities and earthquakes in the area (Yang et al., 2020).

Fault healing is a process that incrementally accumulates energy

* Corresponding author.
E-mail address: gxuwangt@163.com (T. Wang).
Peer review under responsibility of Institute of Rock and Soil Mechanics, Chinese Academy of Sciences.

https://doi.org/10.1016/j.jrmge.2025.02.015
1674-7755/© 2025 Institute of Rock and Soil Mechanics, Chinese Academy of Sciences. Published by Elsevier B.V. This is an open access article under the CC BY license (http://creativecommons.org/licenses/by/4.0/).

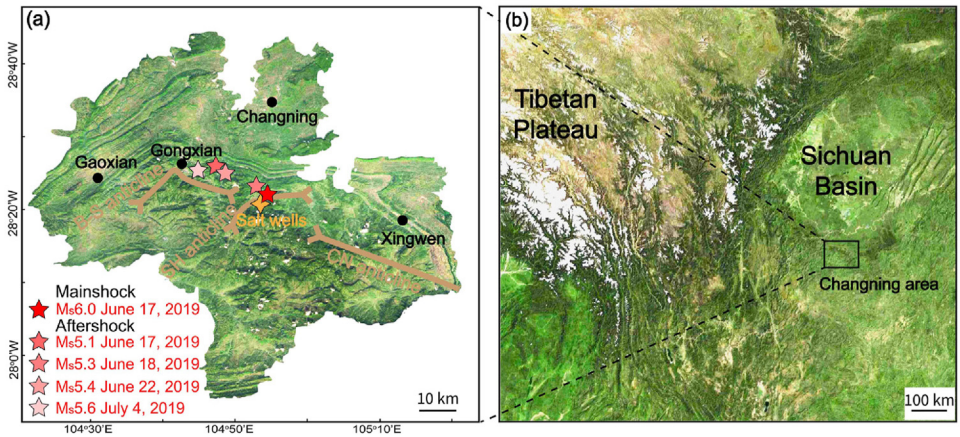

Fig. 1. (a) Topographic map of the Changning area, with the five-pointed stars standing for earthquakes, the yellow four-pointed star denoting salt wells, and the black circles representing the city. "CN", "SH", and "B-S" indicate Changning, Shuanghe, and Baixiangya–Shizitan, respectively (modified from Lei et al., 2019). (b) The Changning area is located in the south of the Sichuan Basin, which is in the east of the Tibetan Plateau.

and restores the shear strength during the inter-seismic period, enabling the fault to withstand repeated earthquake failures (Brace, 1972; Dieterich, 1972). This process involves complex physical and chemical interactions within the fault zone, significantly influencing the magnitude and recurrence interval of sequential earthquakes. Previous laboratory and field data suggest that faults can heal rapidly, as evidenced by observations made approximately 7 months following the Wenchuan earthquake (Tadokoro and Ando, 2002; Xue et al., 2013; Bedford et al., 2023). Notably, in 2019, numerous aftershocks with magnitudes exceeding *Ms*5.0 were recorded in Changning, likely influenced by the rapid healing of the fault (Lei et al., 2019). This phenomenon deviates from Bath's law, a well-established scaling law that typically predicts an average magnitude difference of 1.2 between the shallow mainshock and its significant aftershocks (Båth, 1965). It is imperative to understand the dynamics of frictional healing to elucidate the mechanism underlying the sequence of the *Ms*6.0 earthquake in Changning.

Numerous factors within fault gouge critically affect the frictional healing of faults, including mineral composition (Carpenter et al., 2016), normal stress (Tao and Dang, 2023), temperature (Karner et al., 1997; Yasuhara et al., 2005), and shear velocity (Marone, 1998; Bedford et al., 2023). Halite is notable for its extremely low permeability and damage self-healing characteristics, with plastic deformation possible under relatively low temperatures and pressures (Urai and Spiers, 2017). Extensive research has demonstrated that halite plays a vital role in determining the frictional strength and stability of faults (van den Ende and Niemeijer, 2019; Ikari and Hüpers, 2021). Despite these insights, the specific contributions of halite to fault healing remain comparatively underexplored. The present study investigates the effects of normal stress and shear velocity on the frictional healing behavior of halite gouge by conducting slide-hold-slide (SHS) shear experiments at room temperature and humidity. The objective is to shed light on the healing mechanisms of halite faults across varying normal stresses and shear velocities.

2. Experiment methods

2.1. Sample preparation and testing procedure

In our experiments, halite was used as the sample material, and the X-ray diffraction (XRD) result shows that the halite has a purity >99% (Fig. 2). To prepare the simulated gouge, halite was firstly crushed and then sieved to achieve particle sizes of less than 106 μm, followed by drying the powders at 65 °C for ~24 h to reduce moisture. The experimental setup involved the placement of the lower half of the clamp, as depicted in Fig. 3, into a square mold. Salt rock was evenly distributed on the clamp and leveled to match the height of the mold, with the mass of the salt rock maintained at 15 g. This setup ensured that the gouge was uniformly sandwiched between the stainless steel clamps. Subsequently, the assembly was covered with the upper half of the clamp and positioned in the instrument. The wing edges of the upper clamp half guaranteed that the contact area between the salt rock and the block consistently remained at 5 cm × 5 cm, thus maintaining a constant normal stress.

The shear experiments were performed using a biaxial deformation apparatus (Fig. 3) located at the Key Laboratory of Geotechnical and Underground Engineering of the Ministry of Education, Tongji University, Shanghai, China. This apparatus could flexibly apply the horizontal and vertical loads via the pistons, with the maximum vertical and horizontal forces reaching 100 kN and an accuracy of 0.5 kN. The load cells were installed on the right and upper pistons to record the force, with a sampling frequency of 100 Hz. The displacements could be recorded by the high-precision grating displacement transducers installed on the piston. The whole shear process for each test was controlled by the EDC222 digital controller. Before the shear experiments, the load cells and grating displacement transducers were calibrated using standard calibrators.

A total of seven SHS experiments were carried out at normal stresses of 5–30 MPa, shear velocities of 1–10 μm/s, and hold times of 10–3000 s. The experimental details are shown in Table 1. The normal stress is applied within approximately 10 min, followed by a 5-min waiting period before conducting the shear test steps. Approximately 3 h following the friction experiments, the selected simulated fault gouge samples were scanned using a scanning electron microscope (SEM) (ZEISS Gemini 300).

2.2. Data analysis

In our experiments, the friction coefficient (μ) is defined as the ratio of shear stress (τ) to normal stress (σ_n), which is expressed as

$$\mu = \tau/\sigma_n \tag{1}$$

The friction response during the SHS process can be assessed by frictional healing and creep relaxation (Fig. 4). Throughout the

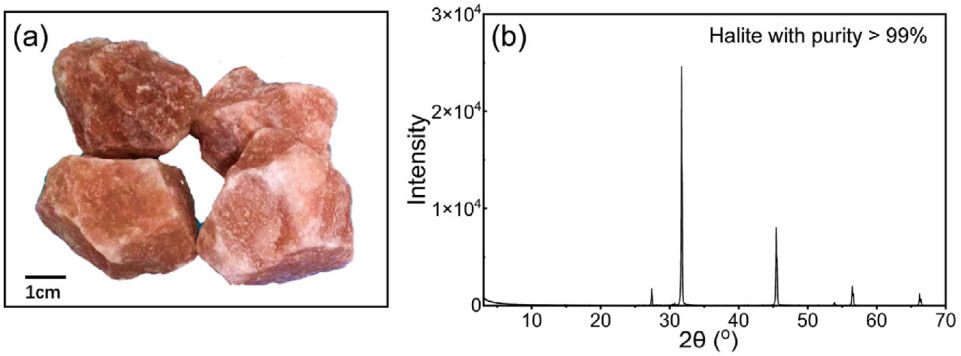

Fig. 2. (a) The photograph of halite samples; and (b) XRD result of the halite powders.

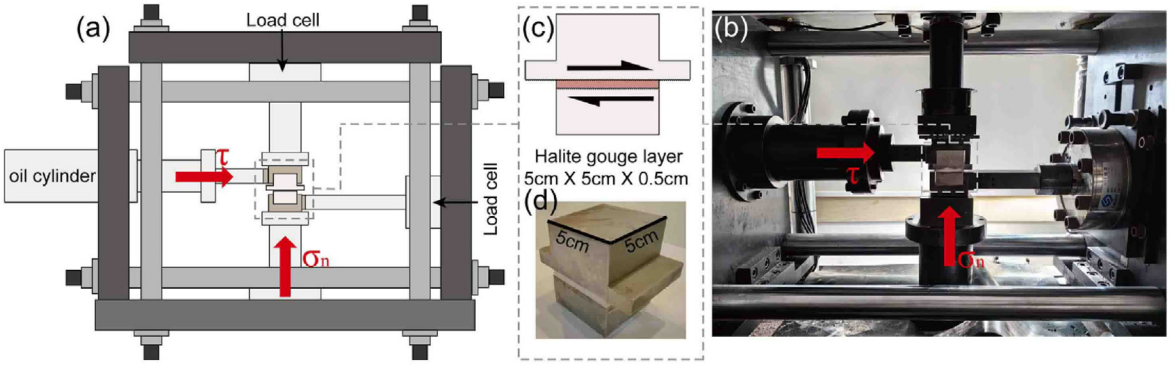

Fig. 3. (a) Schematic of the biaxial deformation apparatus; (b) Photograph of the apparatus; (c) Schematic of the simulated fault gouge assembly; and (d) Photograph of the simulated fault gouge assembly.

Table 1
Experiment matrix.

Experiment No.	Normal stress (MPa)	Shear velocity (μm/s)	Layer thickness (mm)	Hold time (s)
H-5-1	5	1	5	10→30→100→300→1000→3000
H-10-1	10	1	5	10→30→100→300→1000→3000
H-15-1	15	1	5	10→30→100→300→1000→3000
H-20-1	20	1	5	10→30→100→300→1000→3000
H-30-1	30	1	5	10→30→100→300→1000→3000
H-10-3	10	3	5	10→30→100→300→1000→3000
H-10-10	10	10	5	10→30→100→300→1000→3000

holding period, the friction coefficient gradually decreases due to the elastic relaxation experienced by the machinery in conjunction with the creep exhibited by the sample. Upon reloading, the friction coefficient attains a maximum peak before a stable value due to shear strength recovery. Frictional healing ($\Delta\mu$) is determined by subtracting the maximum friction coefficient during re-shearing from the steady-state friction coefficient at the end of the initial shear. Creep relaxation ($\Delta\mu_c$) is calculated as the difference between the steady-state friction coefficient at the beginning of the hold period and its corresponding valley using the following equation:

$$\Delta\mu = \mu_{peak} - \mu_{ss} \tag{2}$$

$$\Delta\mu_c = \mu_{ss} - \mu_{min} \tag{3}$$

where μ_{peak} is the maximum friction coefficient during re-shearing, μ_{ss} is the steady-state friction coefficient at the end of the initial shearing (Fig. 4), and μ_{min} is the minimum friction coefficient during the hold time.

Previous studies have demonstrated a positive correlation between both frictional healing and creep relaxation with the logarithm of time (Dieterich, 1972), as indicated by empirical evidence:

$$\beta = \frac{\Delta\mu}{\log_{10} t_h} \tag{4}$$

$$\beta_c = \frac{\Delta\mu_c}{\log_{10} t_h} \tag{5}$$

where β is the frictional healing rate, and β_c is the creep relaxation rate.

The compaction (Δh_c) of the fault gouge refers to the value of layer thickness decrease during the holding period, while shear dilation (Δh) denotes the subsequent increase in the layer thickness of the fault gouge upon re-shearing.

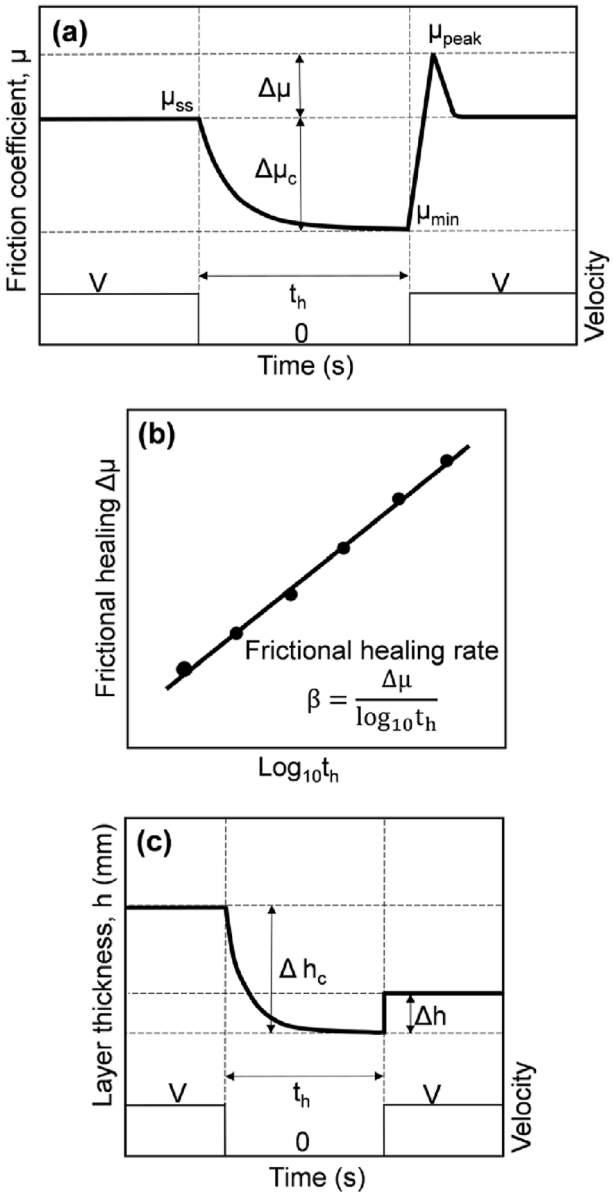

Fig. 4. (a) Schematic of SHS test. Example determinations of (b) frictional healing rate β and (c) frictional compaction Δh_c and dilation Δh.

3. Results

3.1. Frictional strength

Figs. 5 and 6 present schematically the results of seven series of SHS tests under varying normal stresses and shear velocities. During the run-in phase, the friction coefficient initially rises to a first-peak value, then decreases, and stabilizes. And some experiments exhibit pronounced strain hardening behavior during the steady-state sliding stage. In each shear experiment, the first-peak friction coefficient consistently increases with normal stress (Fig. 7a). Conversely, the first-peak friction coefficient exhibits a negative correlation with shear velocity, as illustrated in Fig. 7b and outlined in Table 2. Furthermore, the disparity between the pre- and post-hold steady-state friction coefficients becomes increasingly pronounced under higher normal stresses, as depicted in Figs. 5 and 6. The testing sequence for normal stress variations revealed stable friction coefficients ranging from 0.6501 to 0.9104. Specifically, as

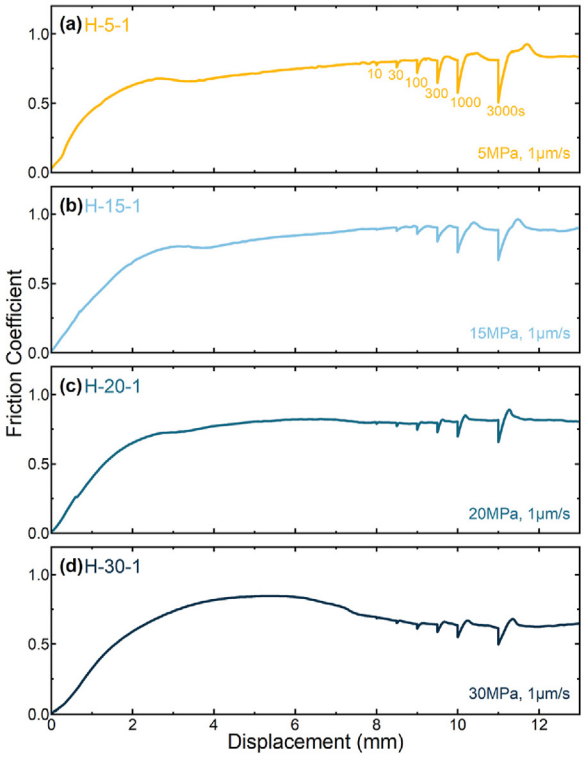

Fig. 5. Plots of the friction coefficient versus load point displacement for (a) H-5-1 ($\sigma_n = 5$ MPa and $v = 1$ μm/s), (b) H-15-1 ($\sigma_n = 15$ MPa and $v = 1$ μm/s1), (c) H-20-1 ($\sigma_n = 20$ MPa and $v = 1$ μm/s), and (d) H-30-1 ($\sigma_n = 30$ MPa and $v = 1$ μm/s), where v is the shear velocity.

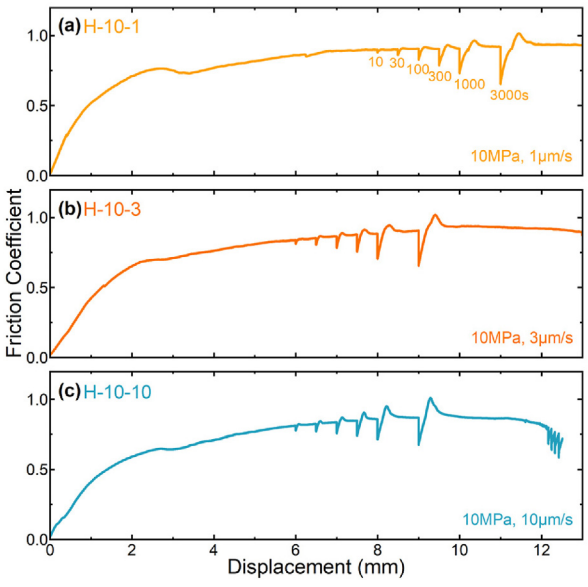

Fig. 6. Plots of the friction coefficient versus load point displacement for (a) H-10-1 ($\sigma_n = 10$ MPa and $v = 1$ μm/s), (b) H-10-3 ($\sigma_n = 10$ MPa and $v = 3$ μm/s), and (c) H-10-10 ($\sigma_n = 10$ MPa and $v = 10$ μm/s). As the shear velocity increases, unstable friction occurs after shear displacements above 11 mm; therefore, experiments at $v = 3$ μm/s and 10 μm/s will commence holding at 6 mm.

the normal stress increases from 5 MPa to 10 MPa, the stable friction coefficient increases (Fig. 7a). However, a further increase in normal stress from 10 MPa to 30 MPa results in a decrease in the stable friction coefficient, which aligns with the findings of

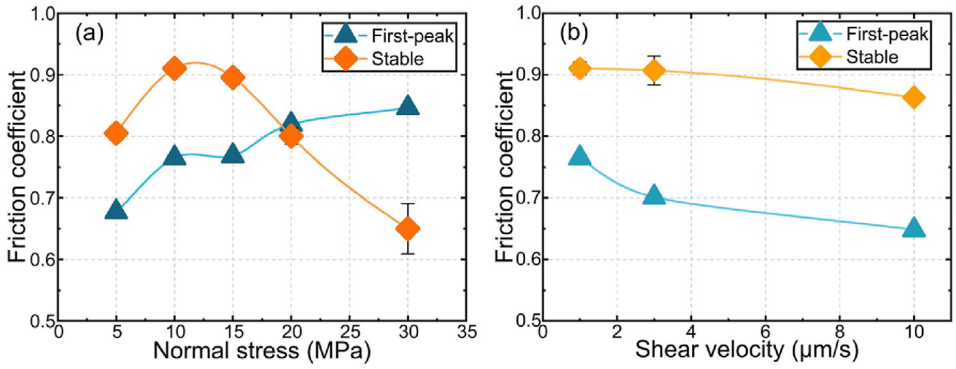

Fig. 7. Variation of the first-peak and stable friction coefficient with (a) normal stress and (b) shear velocity. The black line represents the fluctuation range of error.

Table 2
Experimental data.

Experiment No.	First peak friction coefficient	Stable friction coefficient[a]	Healing rate, β	Relaxation rate, β_c	Total compaction (13 mm) (mm)[b]	Total compaction (11 mm) (mm)[b]
H-5-1	0.6775	0.8051	0.0724	0.1188	3.2099	–
H-10-1	0.7648	0.9104	0.0602	0.0974	3.2083	3.0862
H-15-1	0.7683	0.8957	0.0491	0.0895	3.9202	–
H-20-1	0.8193	0.8005	0.0429	0.0575	3.6986	–
H-30-1	0.8463	0.6501	0.039	0.0446	4.3947	–
H-10-3	0.7013	0.907	0.0608	0.0893	–	3.0932
H-10-10	0.6482	0.8633	0.0759	0.0615	–	2.77304

[a] Stable friction coefficient is calculated as the average of the coefficients measured at 8 mm, 9 mm, and 11 mm, where friction remains relatively stable.
[b] Total compaction (11 mm) and total compaction (13 mm) indicate the compression amounts corresponding to shear displacements of 11 mm and 13 mm, respectively.

Table 3
Frictional healing and creep relaxation for each holding segment.

Experiment No.	$\Delta\mu$ at different hold times						$\Delta\mu_c$ at different hold times					
	10 s	30 s	100 s	300 s	1000 s	3000 s	10 s	30 s	100 s	300 s	1000s	3000 s
H-5-1	0.002	0.005	0.011	0.044	0.068	0.123	0.02	0.041	0.092	0.16	0.235	0.304
H-10-1	0.002	0.009	0.008	0.026	0.058	0.097	0.019	0.039	0.08	0.119	0.178	0.267
H-15-1	0	0.007	0.007	0.018	0.047	0.079	0.008	0.022	0.052	0.101	0.179	0.216
H-20-1	0.001	0.002	0.011	0.021	0.044	0.074	0.011	0.023	0.044	0.069	0.106	0.158
H-30-1	0	0.002	0.008	0.021	0.041	0.066	0.008	0.159	0.034	0.055	0.085	0.118
H-10-3	0.007	0.01	0.019	0.03	0.059	0.109	0.025	0.046	0.08	0.122	0.177	0.249
H-10-10	0.01	0.017	0.032	0.059	0.1	0.144	0.037	0.054	0.08	0.107	0.144	0.191

previous studies on halite and other minerals (Saffer et al., 2001; Saffer and Marone, 2003; Ikari and Hüpers, 2021). Concerning shear velocity, the stable friction coefficients ranged from 0.8368 to 0.9104 as the shear velocity increased from 1 μm/s to 10 μm/s. These findings are also consistent with previous research (Fig. 7b) (Marone, 1998; Marone and Saffer, 2015; van den Ende and Niemeijer, 2019).

3.2. Frictional healing and creep relaxation

Frictional healing is a process that has been widely recognized as the restoration of a fault's shear strength during the inter-seismic period. The findings of this study demonstrate that the frictional healing rate for hold times greater than 100 s is significantly higher than that for hold times less than 100 s, which aligns with the results of previous research on quartz fault gouge at 65 °C (Yasuhara et al., 2005). Additionally, it is observed that the disparity in healing rate before and after 100 s diminishes with increasing normal stress (Fig. 8a and b). Considering the extended duration required for fault healing, the present analysis primarily focuses on hold times exceeding 100 s. The experimental findings on normal stress variations have shown a frictional healing rate ranging from 0.039 to 0.0724. The variations in shear velocity yielded a healing rate of 0.0602–0.0759 (Table 2). The frictional healing rate decreases as the normal stress increases from 5 MPa to 30 MPa, exhibiting a progressive decline until it stabilizes at a nearly constant value (Fig. 9a). In contrast, the healing rate linearly increases with the shear velocity ranging from 1 μm/s to 10 μm/s (Fig. 9b). In summary, the process of frictional healing in salt rock faults is governed by both normal stress and shear velocity. (Figs. 8 and 9).

Creep relaxation refers to the progressive reduction in stress following the cessation of fault slip after an earthquake (Marone, 1991). The phenomenon occurs when the strain energy accumulated within the sample and testing apparatus is released, resulting in a reduced shear stress. The findings of this study indicate that the creep relaxation value diminishes as the normal stress increases from 5 MPa to 30 MPa. Furthermore, an increase in shear velocity is associated with a decrease in the creep relaxation value (Fig. 8). In contrast to the trend observed for frictional healing value versus logarithmic hold times, creep relaxation exhibits a linear increase with logarithmic hold times, aligning with previous measurements conducted on other minerals (Carpenter et al., 2016; Zhang et al.,

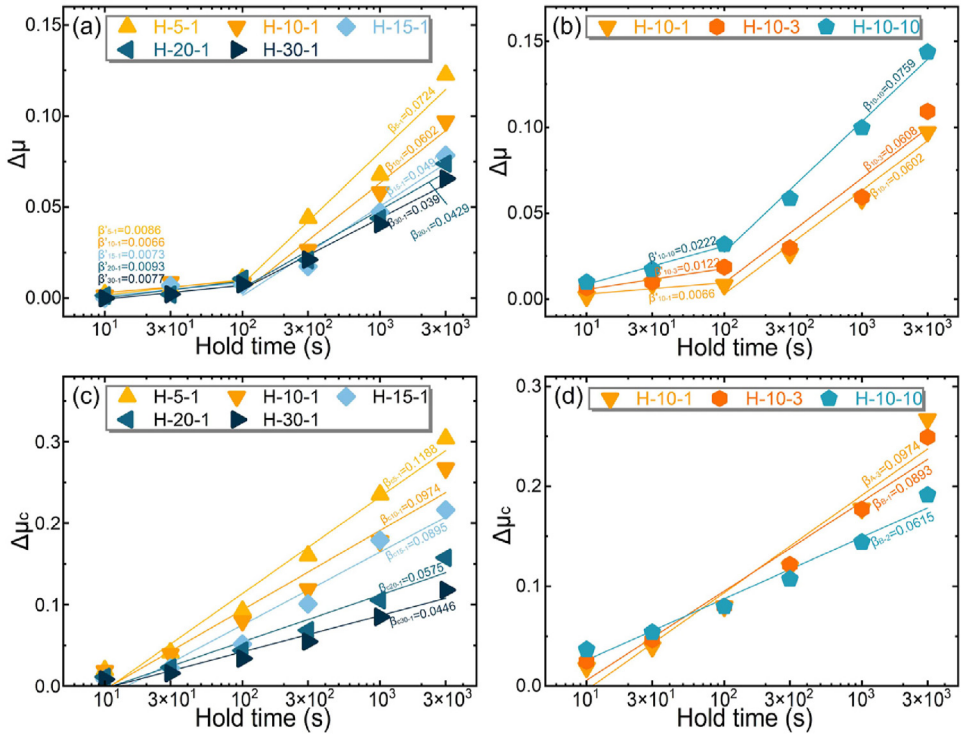

Fig. 8. The frictional healing ($\Delta\mu$) and creep relaxation ($\Delta\mu_c$) plotted against hold time under varying normal stresses (a, c) and shear velocities (b, d). The detailed data are presented in Table 3.

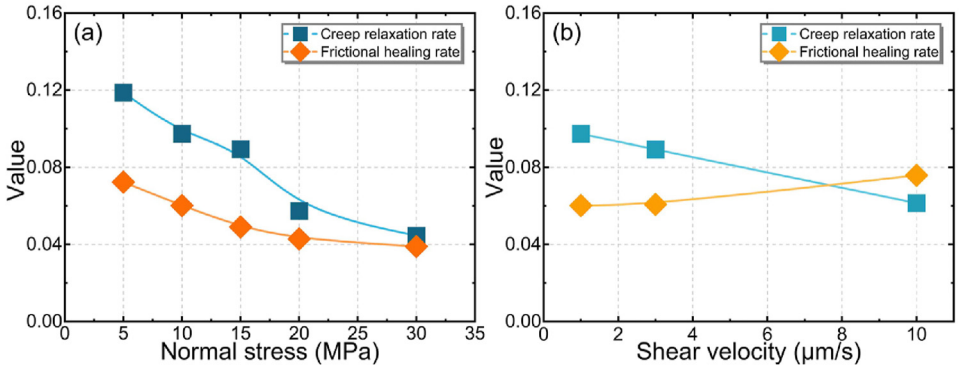

Fig. 9. Variation of frictional healing rate (β) and creep relaxation rate (β_c) with (a) normal stress and (b) shear velocity.

2019). In our tests, creep relaxation rates for changes in normal stress ranged from $\beta_c = 0.0446$ to $\beta_c = 0.1188$, while rates for changes in shear velocity spanned from $\beta_c = 0.0615$ to $\beta_c = 0.0974$ (Table 2). The rate of creep relaxation decreases with the increase of the normal stress, ranging from 5 MPa to 30 MPa. Similarly, it decreases as the shear velocity increases from 1 μm/s to 10 μm/s (Fig. 9).

3.3. Dilation and compaction

The compaction and dilation of fault zones are critical for understanding the seismic cycle (Segall and Rice, 1995). The trend of normalized compaction, when subjected to varying normal stresses and shear velocities, bears a notable resemblance to the normalized dilation trend (Fig. 10). Notably, both compaction and dilation decrease as normal stress increases from 5 MPa to 30 MPa. Furthermore, both trends show an increase with higher shear velocities (Fig. 10). The generated data indicate that compaction and shear dilation approximately follow a linear increase with the logarithm of the hold times, aligning with results from previous studies (Carpenter et al., 2016; Zhang et al., 2019). Total compaction increases proportionally with the normal stress, whereas an increase in shear velocity leads to a reduction in overall compaction (Fig. 11).

3.4. Microstructural observations

SEM is used to investigate the correlation between compaction and lithification with normal stress. As shown in Fig. 12a–c, at $\sigma_n = 5$ MPa, the halite particles are loosely packed and exhibit relatively larger sizes. Only a minute fraction of the particles displays indications of pressure solution attributable to normal stress, and the porosity is at its highest at this stage (Fig. 11a). As the normal stress increases to 10 MPa, the pressure solution effect

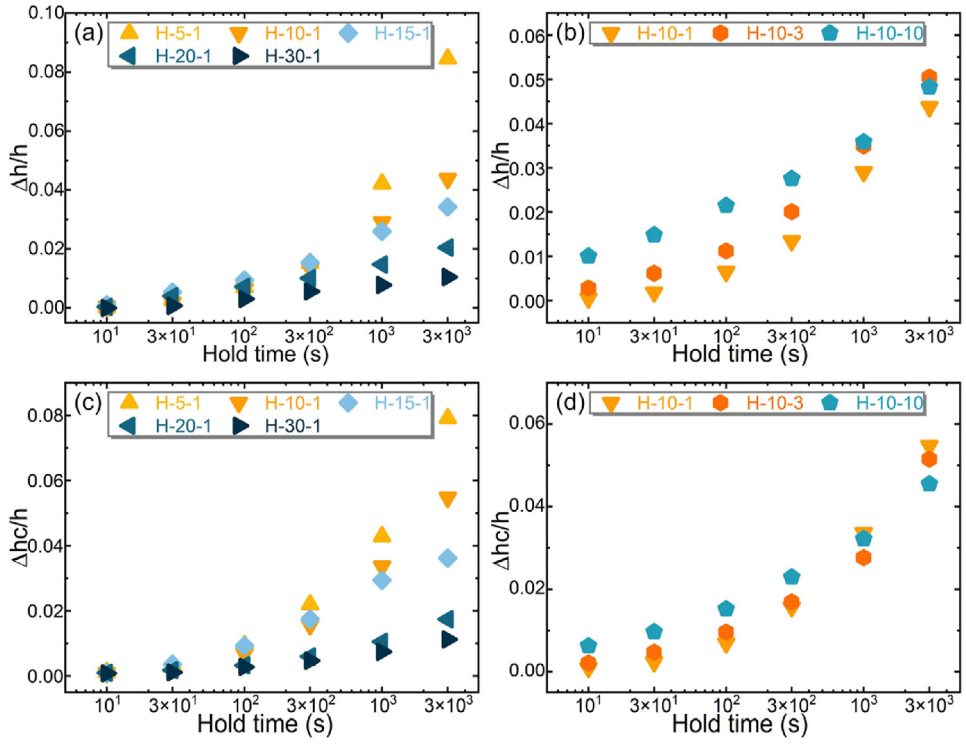

Fig. 10. Volumetric strain data for different hold times at various normal stresses and shear velocities: (a, b) Normalized dilation ($\Delta h/h$) upon re-shearing; and (c, d) Normalized compaction ($\Delta h_c/h$) during holds.

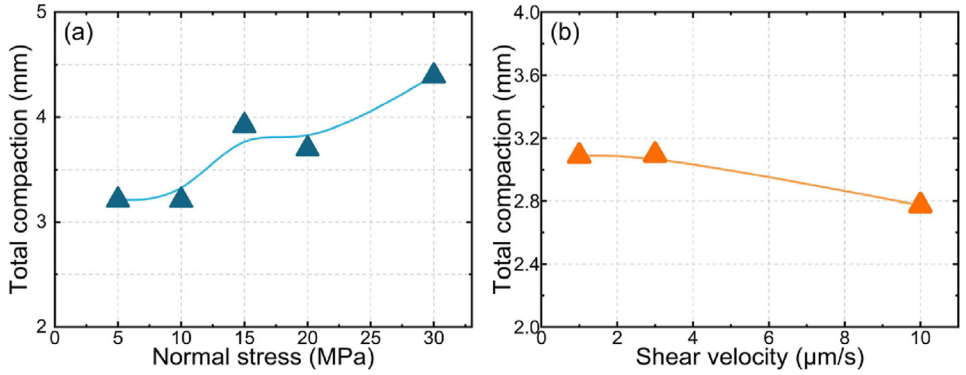

Fig. 11. Variation of total compaction (a) at different normal stresses at a shear displacement of 11 mm and (b) at different shear velocities at a shear displacement of 13 mm.

becomes increasingly pronounced. The fault gouge undergoes tighter compaction, and a cohesive mass is progressively formed. Additionally, more particles show signs of fragmentation (Fig. 12d–f). Under the application of 30 MPa normal stress, both mechanical compaction and pressure solution phenomena become evident, and particles gradually coalesce and bond tightly, eventually forming a structure resembling solid rock. Additionally, shear process induces significant breakage of simulated fault gouge, with the most particle sizes being reduced to below 1 μm (Fig. 12g–i).

4. Discussion

4.1. The effect of lithification

Lithification is a fascinating geological process that transforms loose sediments into solid rock, influenced by factors such as temperature and pressure (Spray, 2016). This process is acknowledged as a driving mechanism for earthquake nucleation (Moore and Saffer, 2001) and facilitates frictional instability (Trütner et al., 2015; Ikari and Hüpers, 2021). The lithification process encompasses physical and chemical mechanisms and plays a crucial role in fault healing (Lisabeth et al., 2024). Both mechanical compaction and pressure solution are significant contributors to fault healing within the lithification process (Angevine et al., 1982; Tao and Dang, 2023). Furthermore, salt rock, notable for its exceptional plasticity and solubility, undergoes lithification even under low temperatures and pressures (Urai and Spiers, 2017). Our experiments indicate the occurrence of mechanical compaction and pressure solution, as evidenced by porosity reduction and inter-particle indentation observed in Fig. 12 (Hafidz et al., 2022).

As the normal stress increases, the salt rock lithification process intensifies, driven by enhanced mechanical and chemical compaction (Evans et al., 1999). Consequently, the simulated fault gouge transforms from a powdered state to a cohesive mass and

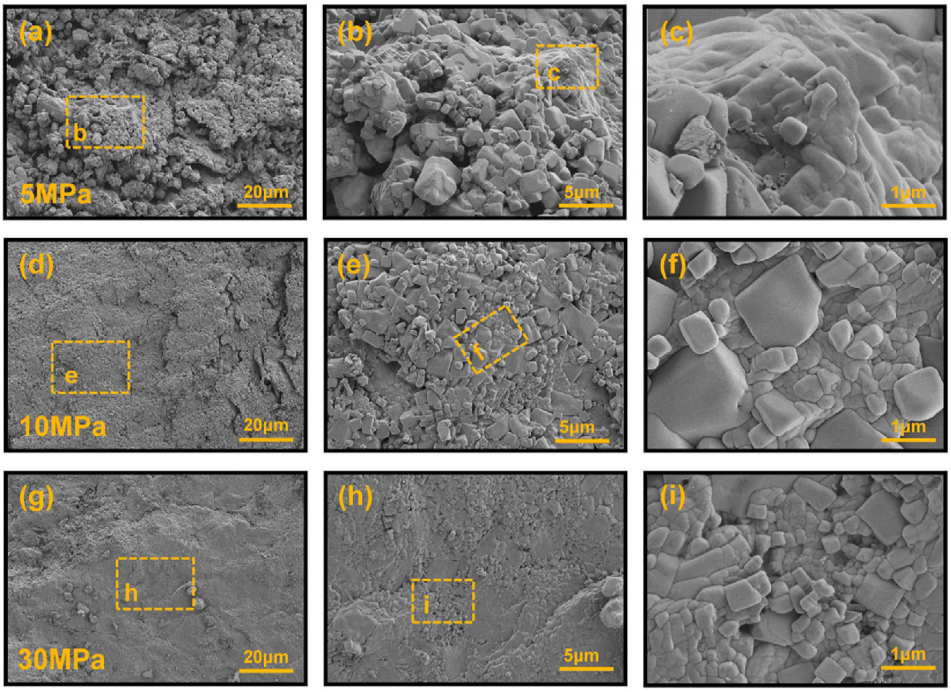

Fig. 12. Microstructures (secondary electron images) of the halite simulated fault gouge after shearing at (a–c) σ_n = 5 MPa, (d–f) σ_n = 10 MPa, and (g–i) σ_n = 30 MPa.

ultimately lithifies into a more complete rock mass (Fig. 12). This transformation resembles the observation reported by Niemeijer et al. (2008), who found that salt rock fault gouge transitions from a clastic state to a cohesive state under the influence of water. Furthermore, it was observed that the post-peak friction coefficient exhibited a more pronounced decrease under higher normal stresses, with a reduction of up to 25% at 30 MPa (Fig. 5d). It is hypothesized that the reduction may be attributed to the fault gouge persisting in a clastic state under lower pressures, resulting in distributed cataclastic flow during shearing (Fig. 12a). As the normal stress increases, the fault gouge undergoes compaction and pressure solution, resulting in the formation of a cohesive mass or a more complete rock mass (Fig. 12d and g). This process subsequently leads to localized frictional sliding after shearing (Giorgetti et al., 2015; Chang et al., 2024). The cohesive mass caused by increasing pressure requires greater resistance to sliding friction during shearing, resulting in a gradual rise in the first-peak friction coefficient. Conversely, an increase in shear velocity reduces the contact time for fault gouge, which subsequently decreases the shear strength of cohesive materials and ultimately results in a diminished first-peak friction coefficient (Fig. 7).

The data presented herein indicate a change in the frictional healing rate at approximately 100 s, aligning with the findings from previous studies on pressure solution in quartz and halite experiments (Yasuhara et al., 2005; Niemeijer et al., 2008). This alteration in the healing rate at 100 s implies a transition in the dominant mechanisms of fault healing. Initially, "Dietrich-type" healing prevails through mechanical compaction, which gives rise to fault closure. Beyond 100 s, the predominant mechanism shifts to pressure solution, which enhances the contact area and bonding strength among particles, thereby facilitating fault healing (Niemeijer et al., 2008). Furthermore, our experimental findings confirm a progressive decrease in the difference between the healing rate before and after 100 s as the normal stress increases (Fig. 8a). It is hypothesized that the impact of pressure solution is minimal during the run-in phase at lower stress. Therefore, during the holding period, this enables fault gouge to have an increased number of contact points, thereby facilitating the pressure solution process. This, in turn, provokes a more significant change in the healing rate (Fig. 12). Conversely, variations in shear velocity do not affect the change in healing rate, maintaining consistency with no evident trend (Fig. 8).

4.2. The relationship between thickness and frictional strength and healing

In our experiments, the simulated fault gouge at 5 MPa remains relatively loose, with only a minor proportion of halite particles undergoing mechanical compaction and pressure solution (Fig. 12b). Consequently, when the normal stress is increased to 10 MPa, both mechanical compaction and pressure solution significantly improve the contact area, triggering a rise in the stable friction coefficient. However, further increases in normal stress only marginally expand the contact area and form a local shear zone, resulting in a decrease in the stable friction coefficient (Fig. 12). The reduction in the stable friction coefficient with increasing shear velocity may be ascribed to the greater shear dilation at higher velocities, which reduces compaction and subsequently diminishes the contact area (Carpenter et al., 2016). Moreover, a faster shear velocity reduces the time required to achieve a given shear distance, which further decreases compaction and reduces the stable friction coefficient (Fig. 11b).

Frictional healing is determined by several factors, including an increase in the contact area between particles, strengthened interparticle contact, and the effects of dilation work (Bos and Spiers, 2002; Yasuhara et al., 2005; Niemeijer et al., 2008; Carpenter et al., 2016). The first two factors are a consequence of fault gouge compaction, while the latter is associated with overcoming dilation through shear stress during fault re-shearing. Previous studies have indicated that up to half of the strength gain in halite can be attributed to dilation work (Niemeijer et al., 2008). The findings of this study establish a direct correlation between

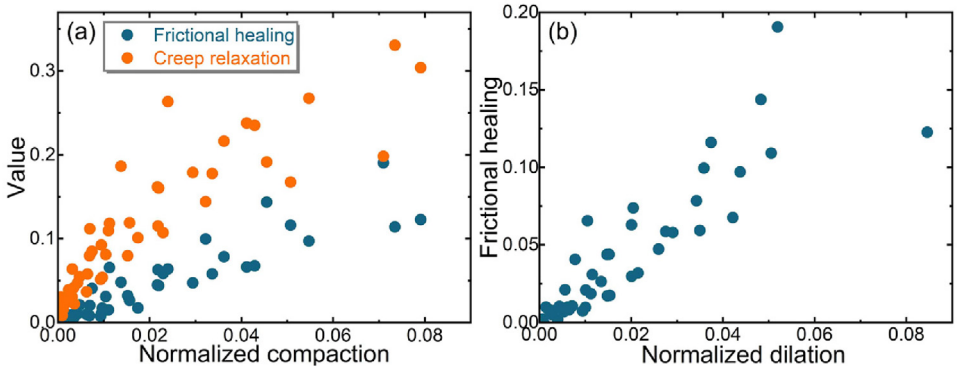

Fig. 13. (a) Relationship between normalized compaction and frictional healing, as well as creep relaxation; and (b) Relationship between normalized dilation and frictional healing.

frictional healing and the normalization of compaction and dilation, underscoring the concurrent influence of these three mechanisms in halite (Fig. 13a). The reduction in compaction and dilation values induces a decrease in frictional healing values during the variation of normal stress from 5 MPa to 30 MPa (Fig. 10a and c). Additionally, an increase in shear velocity from 1 μm/s to 10 μm/s enhances dilation during re-shearing, which in turn increases the frictional healing rate (Marone, 1998). Creep relaxation occurs due to the compaction of fault gouge, which induces creep within the sample and subsequently alleviates stress. Our experiments further demonstrate a proportional relationship between normalized compaction and creep relaxation (Fig. 13b).

4.3. Implications for induced earthquakes

Our findings signify that when considering only the effect of effective normal stress, the increase in fault depth of salt rock and the reduction in fluid pressure caused by fluid diffusion lead to an increase in effective normal stress, consequently decreasing the frictional healing rate. However, once the effective stress reaches a certain threshold, such as 20 MPa in this study, further increases in effective normal stress only result in a slight reduction in the frictional healing rate (Giorgetti et al., 2015). Previous studies have indicated that when considering only fault slip velocity, the healing effect of the fault will be countered by post-seismic slip when the shear velocity exceeds critical sliding velocity (Marone, 1998). Meanwhile, during fault activation, an increase in shear velocity contributes to rapid healing of the fault during inter-seismic periods (Bedford et al., 2023). This phenomenon is consistent with the experimental results of this study (Fig. 9b).

Faults containing minerals with higher frictional strength, greater shear dilation, and stronger healing are more prone to velocity weakening, making them more likely to experience repeated earthquakes (Ikari et al., 2011; Trütner et al., 2015; Ikari and Hüpers, 2021). When a higher frictional strength fault slips, it encounters greater resistance, resulting in enhanced stress accumulation. Once this stress exceeds the fault's friction strength, it may release more energy, leading to larger earthquake magnitudes. As illustrated in Fig. 14a, the stable friction coefficient of halite surpasses that of other minerals (Carpenter et al., 2016; Zhang et al., 2019; Cao et al., 2024). Furthermore, its unique property of being readily lithified further increases this friction coefficient, thereby contributing to fault instability. Near the epicenter of the *Ms*6.0 earthquake in Changning, a notable presence of salt rock was observed, probably increasing the friction strength of the fault (He et al., 2019). This could result in a more pronounced accumulation of energy, thereby facilitating the occurrence of the Changning *Ms*6.0 earthquake.

A comparison of our data with previous findings on the healing rates of various minerals reveals that the healing rate of halite during the initial mechanical compaction-dominated phase aligns with the healing rates of other minerals. However, under prolonged pressure solution-dominated conditions, the healing rate of halite is significantly greater than that of other minerals in previous studies (Fig. 14b) (Yasuhara et al., 2005; Carpenter et al., 2016; Zhang et al., 2019; Cao et al., 2024). This reveals that the healing rate of halite during the inter-seismic period is relatively high, enabling faster energy accumulation. Consequently, faults containing salt rock can accumulate energy more quickly after an earthquake, resulting in larger aftershock magnitudes. Following the *Ms*6.0 earthquake in Changning, multiple aftershocks of $Ms \geq 5.0$ occurred, a

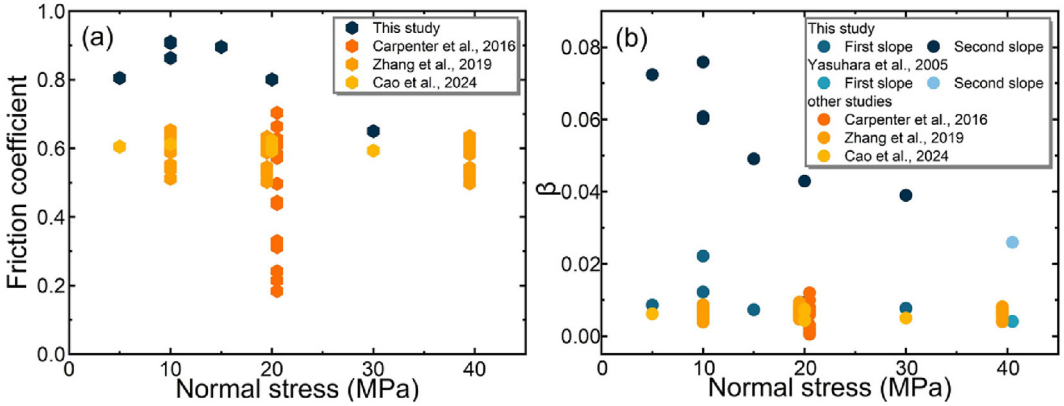

Fig. 14. Variation of (a) stable friction coefficient and (b) frictional healing rate (β) with normal stress. Comparing the data obtained in this study with the stable friction coefficient and friction healing rate of various minerals in previous studies, it can be found that halite has a stronger friction coefficient and friction healing rate.

phenomenon that does not align with traditional Bath's law (Båth, 1965). The presence of salt rock and its elevated healing rate may offer a plausible explanation for this observed behavior.

5. Conclusions

A systematic study of the SHS experiment in halite is performed to investigate the effect of normal stress and shear velocity on frictional strength and frictional healing properties of halite gouge. The following conclusions were drawn in this experiment.

(1) The frictional strength and rate of frictional healing in halite gouge exceed those of other minerals, suggesting a significant influence of halite on the Changning *Ms*6.0 earthquake. Faults containing halite are more susceptible to larger induced earthquakes, resulting in aftershocks with magnitudes exceeding those typically observed in induced seismicity.
(2) As the normal stress increases from 5 MPa to 30 MPa, the first-peak friction coefficient exhibits a gradual upward trend, whereas the stable friction coefficient initially increases and then decreases. Furthermore, the friction healing rate shows a progressive decline with the rise in normal stress.
(3) The increase in shear velocity from 1 μm/s to 10 μm/s facilitates fault healing during hold times and reduces the shear strength.
(4) The healing of halite faults involves both mechanical compaction and pressure solution mechanisms, with a shift in the dominant mechanism occurring at 100 s. Furthermore, the lithification of halite significantly influences the frictional strength, frictional healing, and creep relaxation.

CRediT authorship contribution statement

Junjie Wei: Writing – original draft, Visualization, Methodology, Investigation, Formal analysis, Data curation, Conceptualization. **Tuo Wang:** Writing – review & editing, Supervision, Project administration, Conceptualization. **Fengshou Zhang:** Writing – review & editing, Supervision, Resources, Funding acquisition.

Declaration of competing interest

The authors declare that they have no known competing financial interests or personal relationships that could have appeared to influence the work reported in this paper.

Acknowledgments

This work is supported by the National Key Research and Development Project (Grant No. 2023YFE0110900) and the National Natural Science Foundation of China (Grant Nos. 42320104003 and 42077247). We are grateful for valuable suggestions on experimentation and writing from Mengke An, and significant contribution from Lu Wang in designing the stainless steel clamps.

References

Angevine, C.L., Turcotte, D.L., Furnish, M.D., 1982. Pressure solution lithification as a mechanism for the stick-slip behavior of faults. Tectonics 1 (2), 151–160.
Anyiam, U.O., Qian, J.W., Tan, Y.Y., Zhang, H.J., 2024. Comprehensive seismic evidence for the inducing mechanism of the extremely shallow 2019 Changning *Ms* 6.0 earthquake by solution salt mining, Sichuan Basin, China. Geology 52 (6), 441–446.
Atkinson, G.M., Eaton, D.W., Igonin, N., 2020. Developments in understanding seismicity triggered by hydraulic fracturing. Nat. Rev. Earth Environ. 1 (5), 264–277.
Båth, M., 1965. Lateral inhomogeneities of the upper mantle. Tectonophysics 2 (6), 483–514.
Bedford, J.D., Hirose, T., Hamada, Y., 2023. Rapid fault healing after seismic slip. J. Geophys. Res. Solid Earth 128 (6), e2023JB026706.
Bos, B., Spiers, C.J., 2002. Fluid-assisted healing processes in gouge-bearing faults: insights from experiments on a rock analogue system. Pure Appl. Geophys. 159 (11–12), 2537–2566.
Brace, W.F., 1972. Laboratory studies of stick-slip and their application to earthquakes. Tectonophysics 14 (3–4), 189–200.
Cao, S.T., Zhang, F.S., An, M.K., Yasuhara, H., 2024. Effects of particle size and normal stress on the frictional stability and healing of simulated basalt gouges: implications for lunar seismicity. Rock Mech. Rock Eng. 57 (12), 10895–10910.
Carpenter, B.M., Ikari, M.J., Marone, C., 2016. Laboratory observations of time-dependent frictional strengthening and stress relaxation in natural and synthetic fault gouges. J. Geophys. Res. Solid Earth 121 (2), 1183–1201.
Chang, C.R., Noda, H., Hamada, Y., Huang, C., Ma, T., Wang, G.H., Yamaguchi, T., 2024. Comminution-induced transient frictional behavior in sheared granular halite. Geophys. Res. Lett. 51 (21), e2024GL109645.
Dieterich, J.H., 1972. Time-dependent friction in rocks. J. Geophys. Res. 77 (20), 3690–3697.
Ellsworth, W.L., 2013. Injection-induced earthquakes. Science 341 (6142), 1225942.
Evans, B., Bernabé, Y., Zhu, W.L., 1999. Evolution of pore structure and permeability of rocks in laboratory experiments. In: Growth, Dissolution and Pattern Formation in Geosystems. Springer, Dordrecht, Netherlands, pp. 327–344.
Giorgetti, C., Carpenter, B.M., Collettini, C., 2015. Frictional behavior of talc-calcite mixtures. J. Geophys. Res. Solid Earth 120 (9), 6614–6633.
Hafidz, A., Kinoshita, N., Yasuhara, H., 2022. Effect of permeants on fracture permeability in granite under hydrothermal conditions. Rock Mech. Bull. 1 (1), 100007.
He, D.F., Lu, R.Q., Huang, H.Y., Wang, X.S., Jiang, H., Zhang, W.K., 2019. Tectonic and geological background of the earthquake hazards in Changning shale gas development zone, Sichuan Basin, SW China. Pet. Explor. Dev. 46 (5), 993–1006.
Ikari, M.J., Hüpers, A., 2021. Velocity-weakening friction induced by laboratory-controlled lithification. Earth Planet Sci. Lett. 554, 116682.
Ikari, M.J., Marone, C., Saffer, D.M., 2011. On the relation between fault strength and frictional stability. Geology 39 (1), 83–86.
Karner, S.L., Marone, C., Evans, B., 1997. Laboratory study of fault healing and lithification in simulated fault gouge under hydrothermal conditions. Tectonophysics 277 (1–3), 41–55.
Lei, X.L., Wang, Z.W., Su, J.R., 2019. Possible link between long-term and short-term water injections and earthquakes in salt mine and shale gas site in Changning, south Sichuan Basin, China. Earth Planet. Phys. 3 (6), 510–525.
Li, M.L., Zhang, F.S., Wang, S.Y., Dontsov, E., Li, P.C., 2024. DEM modeling of simultaneous propagation of multiple hydraulic fractures across different regimes, from toughness- to viscosity-dominated. Rock Mech. Rock Eng. 57 (1), 481–503.
Li, Z.Q., Ma, X.D., Kong, X.Z., Saar, M.O., Vogler, D., 2023. Permeability evolution during pressure-controlled shear slip in saw-cut and natural granite fractures. Rock Mech. Bull. 2 (2), 100027.
Lisabeth, H., DePaolo, D.J., Pester, N.J., Christensen, J.N., 2024. Concurrent measurement of strain and chemical reaction rates in a calcite grain pack undergoing pressure solution: evidence for surface-reaction controlled dissolution. Geochim. Cosmochim. Acta. 385, 184–198.
Marone, C., 1998. The effect of loading rate on static friction and the rate of fault healing during the earthquake cycle. Nature 391 (6662), 69–72.
Marone, C., 1991. A note on the stress-dilatancy relation for simulated fault gouge. Pure Appl. Geophys. 137 (4), 409–419.
Marone, C., Saffer, D.M., 2015. The mechanics of frictional healing and slip instability during the seismic cycle. In: Treatise on Geophysics, second ed. Elsevier, Amsterdam, Netherlands, pp. 111–138.
Moore, J.C., Saffer, D., 2001. Updip limit of the seismogenic zone beneath the accretionary prism of southwest Japan: an effect of diagenetic to low-grade metamorphic processes and increasing effective stress. Geology 29 (2), 183.
Niemeijer, A., Marone, C., Elsworth, D., 2008. Healing of simulated fault gouges aided by pressure solution: results from rock analogue experiments. J. Geophys. Res. Solid Earth 113 (B4), B04204.
Saffer, D.M., Frye, K.M., Marone, C., Mair, K., 2001. Laboratory results indicating complex and potentially unstable frictional behavior of smectite clay. Geophys. Res. Lett. 28 (12), 2297–2300.
Saffer, D.M., Marone, C., 2003. Comparison of smectite- and illite-rich gouge frictional properties: application to the updip limit of the seismogenic zone along subduction megathrusts. Earth Planet Sci. Lett. 215 (1–2), 219–235.
Schultz, R., Skoumal, R.J., Brudzinski, M.R., Eaton, D., Baptie, B., Ellsworth, W., 2020. Hydraulic fracturing-induced seismicity. Rev. Geophys. 58 (3), 1–43.
Segall, P., Rice, J.R., 1995. Dilatancy, compaction, and slip instability of a fluid-infiltrated fault. J. Geophys. Res. Solid Earth 100 (B11), 22155–22171.
Snæbjörnsdóttir, S., Sigfússon, B., Marieni, C., Goldberg, D., Gislason, S.R., Oelkers, E.H., 2020. Carbon dioxide storage through mineral carbonation. Nat. Rev. Earth Environ. 1 (2), 90–102.
Spray, J.G., 2016. Lithification mechanisms for planetary regoliths: the glue that binds. Annu. Rev. Earth Planet Sci. 44 (1), 139–174.
Sun, X.L., Yang, P.T., Zhang, Z.W., 2017. A study of earthquakes induced by water injection in the Changning salt mine area, SW China. J. Asian Earth Sci. 136, 102–109.

Tadokoro, K., Ando, M., 2002. Evidence for rapid fault healing derived from temporal changes in S wave splitting. Geophys. Res. Lett. 29 (4), 1047.
Tao, K., Dang, W.G., 2023. Frictional behavior of quartz gouge during slide-hold-slide considering normal stress oscillation. Int. J. Coal Sci. Technol. 10 (1), 1–14.
Trütner, S., Hüpers, A., Ikari, M.J., Yamaguchi, A., Kopf, A.J., 2015. Lithification facilitates frictional instability in argillaceous subduction zone sediments. Tectonophysics 665, 177–185.
Urai, J.L., Spiers, C.J., 2017. The effect of grain boundary water on deformation mechanisms and rheology of rocksalt during long-term deformation. In: The Mechanical Behavior of Salt – Understanding of THMC Processes in Salt: Proceedings of the 6th Conference (SaltMech6). CRC Press, London, UK, pp. 149–158.
van den Ende, M.P.A., Niemeijer, A.R., 2019. An investigation into the role of time-dependent cohesion in interseismic fault restrengthening. Sci. Rep. 9 (1), 9894.
Xue, L., Li, H.B., Brodsky, E.E., et al., 2013. Continuous permeability measurements record healing inside the Wenchuan earthquake fault zone. Science 340 (6140), 1555–1559.
Yang, Y.H., Hu, J.C., Chen, Q., et al., 2020. Shallow slip of blind fault associated with the 2019 *Ms*6.0 Changning earthquake in fold-and-thrust belt in salt mines of Southeast Sichuan, China. Geophys. J. Int. 224 (2), 909–922.
Yasuhara, H., Marone, C., Elsworth, D., 2005. Fault zone restrengthening and frictional healing: the role of pressure solution. J. Geophys. Res. Solid Earth 110 (B6).
Zhang, B., Lei, J.S., Zhang, G.W., 2020. Seismic evidence for influences of deep fluids on the 2019 Changning Ms 6.0 earthquake, Sichuan basin, SW China. J. Asian Earth Sci. 200, 104492.
Zhang, F., An, M., Zhang, L., Fang, Y., Elsworth, D., 2019. The role of mineral composition on the frictional and stability properties of powdered reservoir rocks. J. Geophys. Res. Solid Earth 124 (2), 1480–1497.

Dr. Tuo Wang obtained his PhD degree in civil engineering in 2021 from Tongji University, China. Currently, he is a postdoctoral fellow at the Hong Kong Polytechnic University. Dr. Wang's research is focused on the coupling of multi-physical fields in deep-earth and deep-sea energy extraction and carbon sequestration. He has participated in several geotechnical engineering projects, including the National Natural Science Foundation. To date, he has published approximately 20 technical papers in geotechnical engineering.